Darnbrough, J., Roebuck, B., & Flewitt, P. (2015). The influence of temperature and grain boundary volume on the resistivity of nanocrystalline nickel. Journal of Applied Physics, 118(18), [184302]. DOI: 10.1063/1.4935290

AIP | Journal of Applied Physics

The influence of temperature and grain boundary volume on the resistivity of nanocrystalline nickel

J. E. Darnbrough, B. Roebuck, and P. E. J. Flewitt

Citation: Journal of Applied Physics **118**, 184302 (2015); doi: 10.1063/1.4935290
View online: http://dx.doi.org/10.1063/1.4935290
View Table of Contents: http://scitation.aip.org/content/aip/journal/jap/118/18?ver=pdfcov
Published by the AIP Publishing

The influence of temperature and grain boundary volume on the resistivity of nanocrystalline nickel

J. E. Darnbrough,[1,a)] B. Roebuck,[2] and P. E. J. Flewitt[1]
[1]*Interface Analysis Centre, School of Physics, University of Bristol, H. H. Wills Physics Laboratory, Tyndall Avenue, Bristol, BS8 1TL, United Kingdom*
[2]*National Physical Laboratory, Hampton Rd, Teddington, Middlesex, TW11 0LW, United Kingdom*

(Received 13 August 2015; accepted 26 October 2015; published online 11 November 2015)

The thermal stability and modes of recrystallisation of nanocrystalline nickel has been observed through a conduction-based non-destructive test. Resistivity measurements have been utilised to quantify grain boundary volume fraction and microstructure. This observation makes clear the distinction of the factors that contribute to resistivity and demonstrates that these contributions are related to microstructure, either directly or in-directly. In static systems, the contribution of ordered grains and low-order grain boundary atomic arrangements in small grained material has been measured and correlated with resistivity. Measurements of *in-situ* resistivity conducted at high temperature gives changes with time which are related to grain growth, during heat treatment. This shows that resistivity can be used as a technique for observing the microstructure and grain growth of small grained material. © *2015 AIP Publishing LLC*.
[http://dx.doi.org/10.1063/1.4935290]

I. INTRODUCTION

For single phase nanocrystalline metals and alloys, it has been demonstrated that the grain size is important in controlling the physical, electrical, and mechanical properties.[1,2] Thus, it is of great interest to develop an understanding and quantification of grain structure for such bulk materials. The relationship of voltage and associated current conducting through a material gives a measurable response that is indicative of the microstructure of the conduction volume, electrical resistivity. However, it is important to understand the fabrication processes that have been adopted to prepare each nano-scale polycrystalline material and overall impurity element content in this case specifically sulpher.[19,20] Electron interactions provide resistance to electric current, due to scattering events with phonons, other electrons and crystal defects impeding the transport of electrons.[3] Although there is a good understanding of the electronic structure of relatively simple metals to make exact calculations of properties associated with electron transport, electrical resistivity becomes more complex. Ziman provides an overview of the mechanisms by which electrons are transported through a material and scattered by phonons, crystal lattice imperfections, and impurity atoms.[4,21] Deconvoluting these effects and utilising them for investigating conduction through a material requires understanding of the scattering providence. The amount of scattering from phonons is related to the temperature of the material, the electron-electron scattering which is dependent on the electron density in the material and the scattering from crystal defects which is dependent on the density and arrangement of the defects.[5] The predominant defect in an unstrained small grained polycrystalline system is the grain boundary, the volume of which is proportional to the inverse of the grain size. A fully dense polycrystalline single phase material with an unchanging average grain boundary width has an increasing proportion of grain boundary volume fraction with decreasing grain size. Modeling a uni-modal grain sized microstructure as a 3D tessellating truncated octahedron, based on the Kelvin tetradecahedron,[6] allows G, the relative proportion of grain volume to the total volume (inverse of B the proportion of grain boundary volume $B = 1 - G$) to be written mathematically as the following equation, where the relationship to grain radius, r, and grain boundary width w, is given in the full derivation (see Appendix)

$$G = \frac{r^3}{\left(r + \frac{w}{2}\right)^3}. \quad (1)$$

In this paper, we consider measurements of resistivity undertaken when nanocrystalline nickel specimens are subject to isothermal heat treatment at high temperatures. The results can be correlated quantitatively with the growth of the grains over time. Overall, the resistivity technique provides a method for monitoring grain growth when applied to small grain size polycrystalline materials.

II. THEORY

Resistivity as stated above is the summation of scattering from a number of effects with thermal, T, and defect structure, ϕ, the predominant contributions. Writing this mathematically allows the role of crystal defects to be evaluated for constant temperature and constant chemical composition (no change in electron density); any variation in total resistivity, $\rho_{total}(T, \phi)$, arises from a change in defect structure, as follows:

a)Electronic mail: J.E.Darnbrough@bristol.ac.uk

$$\begin{aligned}\rho_{total}(T,\phi) &= \rho_{ee} + \rho_{phonon}(T,\phi) + \rho_{defect}(\phi)\\ &= \rho_{ee} + \underbrace{G\rho_{lattice}(T) + B\rho_{non-lattice}(T)}_{\text{phonon contributors}} + \underbrace{G\rho_{grain} + B\rho_{gb}}_{\text{defect contributors}}\\ &= \rho_{ee} + \underbrace{G(\rho_{lattice}(T) + \rho_{grain})}_{\text{Grain Contribution}} + \underbrace{B(\rho_{non-lattice}(T) + \rho_{gb})}_{\text{Grain Boundary Contribution}}\\ &= \rho_{ee} + G(\rho_{lattice}(T) - \rho_{non-lattice}(T) + \rho_{grain} - \rho_{gb}) + \rho_{gb} + \rho_{non-lattice}(T). \end{aligned} \quad (2)$$

This equation relates the electron (ρ_{ee}), phonon ($\rho_{lattice}$ and $\rho_{non-lattice}$), and defect (ρ_{grain} and ρ_{gb}) contributions to the total resistivity. By rearranging Eq. (2) and expanding the contributions allow resistivity for a volume of microstructure that contains regions of order, grains ρ_{grain}, or low-order, grain boundaries ρ_{gb}, to be identified. Inherent in this is the assumption that all grain interiors are alike with a mean response in phonon and defect resistivity which is representative of all grains in a poly-crystal; the same applies to the total grain boundary volume. This assumes that the effect of composition, electron-electron scattering, ρ_{ee}, due to electron density, is constant and any contribution due to the small electric field in the conducting material is very small. The expanded form of Eq. (2) shows that the separation of phonon and defect contributions is dependent on the relative volumes of grain interior, G, and grain boundary, B. Moreover, the total resistivity is linearly proportional to the fraction of grain interior and as temperature, T, is varied, the size of resistivity change would depend on the proportion of grain interior to grain boundary.

III. EXPERIMENTAL

A. Material

We consider nanopolycrystalline (nc) nickel which has been shown to exhibit unusual grain coarsening characteristics.[7,20] Electrodeposited bulk nc nickel containing 280 ppm impurity sulphur has a unique microstructural evolution during heat treatment above 758 K, resulting in large abnormal planar grains in a stable matrix of smaller grains.[7,20] The as-received 46.2 ± 2.6 nm grain size material initially coarsens to produce a uni-modal grain size of ~550 nm diameter and then stagnates producing subsequently a stable microstructure from which abnormal grain growth eventually occurs, resulting in a bi-modal grain size distribution. The abnormal grains in this material observed as micrometre length-scale planar faceted grains grow from an array of the stagnant grains. Nanocrystalline nickel was produced by electrodeposition with an impurity level of 280 ppm sulphur. A previous investigation has characterised the virgin grain size as 46.2 ± 2.6 nm diameter through a combination of transmission electron bright and dark field imaging and diffraction and X-ray diffraction.[20] At temperatures above 573 K, this exhibits grain stagnation of coarsening at an average grain size ~550 nm. With heat treatment above 758 K, abnormal planar faceted growth is observed from a stagnant grain size microstructure as displayed in Figure 1. All grain size and abnormal grain volume data are measured from a combination of these two imaging modes for a range of heat treatment conditions. Below this heat treatment temperature of 758 K, normal grain coarsening kinetics is observed. Thorough investigation using sub-surface high-resolution SEM imaging of focused ion beam milled sections and TEM thin foils showed a fully dense material with no sub-micrometre voids and few dislocations. The XRD results showed little strain in the material which supports that there is no significant defect structure within the grains. In addition Darnbrough and Flewitt have explained that the role of impurity sulphur and its importance for grain growth.[20]

B. Discrete-time four-point probe experiments

A simple four-point set-up is utilised to measure the resistivity of a material by applying a current and measuring the subsequent potential difference across a known length specimen with a fixed cross-section, Figure 2(a). By measuring the potential, V ± 1μV, with varying current, I ± 1 mA, the linear relationship with resistance confirms no change in resistivity due to either temperature or microstructural

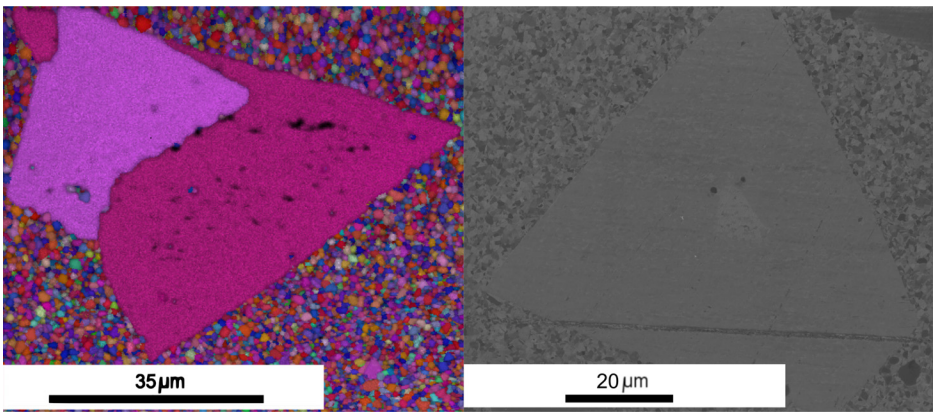

FIG. 1. (a) Typical focused ion beam and electron back-scatter detection images of heat treated nc Nickel displaying the bi-modal microstructure with stagnant ~550 nm matrix and large planar abnormal grains.

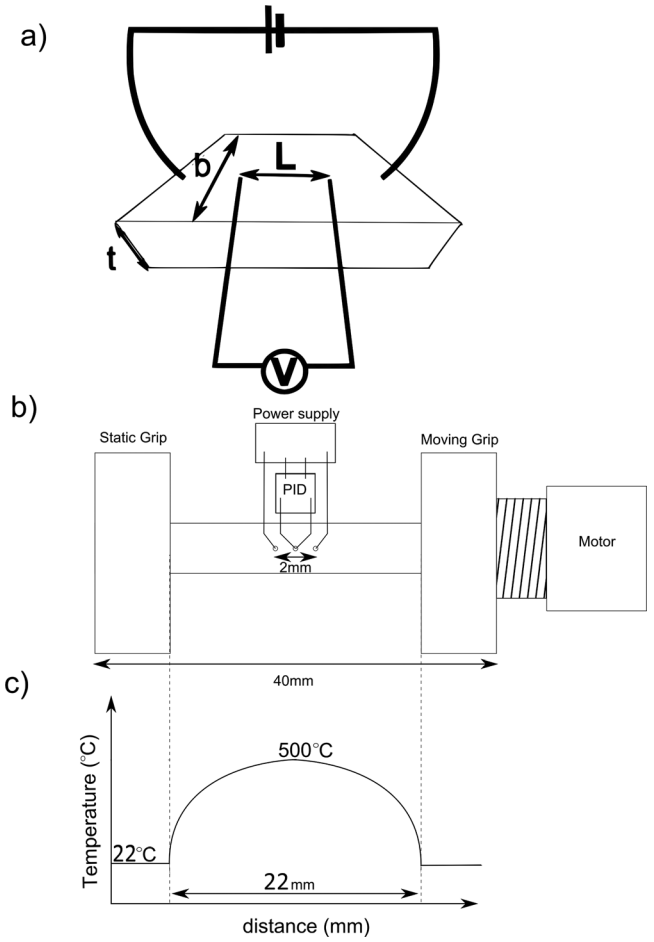

FIG. 2. (a) Figure showing an arrangement where a specimen of known thickness, t, and width, b, is connected to a current generator and a voltmeter via platinum wires which are spot-welded to the specimen. L is the separation of the connectors over which the potential difference is measured, where A is the area calculated from the multiplication of b and t. $R = \frac{V}{I} = \frac{\rho L}{A}$. (b) Schematic of the NPL, ETMT rig (not to scale) showing the central test specimen between grips, (c) an example of a temperature gradient with the relative location within the specimen displayed and the location for the thermocouple and the electrical contacts.

change.[8] This experimental arrangement has been used over a range of temperatures, 77 K to 773 K. Working with low temperatures (77 K, submersion in liquid nitrogen), consideration of the effect of thermal gradients across conductors and electrical junctions is required. Thermal electromotive force (emf) can be produced by the thermoelectric (Seebeck) effect, when a disparity in temperature occurs between different metals in contact.[9] To conduct a resistivity measurement at 77 K, the specimen and spot-welded Pt wire connections have to be submerged in liquid nitrogen. The length of the Pt wire connections to both the current generator and voltmeter have to ensure that both sets of junctions are in a stable thermal environment and reduce any experimental noise.

C. Continuous-time ElectroThermoMechanical Test (ETMT) rig experiments

A constant high temperature can cause changes in the microstructure of a polycrystalline single phase metal through grain growth and the removal of dislocations.[10–12] A concurrent physical effect of passing a large current through a material is to produce "resistive heating." This effect is utilised to hold a test specimen at a constant temperature, using a thermocouple and a proportional integral derivative (PID) feedback loop, heated by the high current. Measuring current and voltage allows the resistance of a specimen with a known volume to be determined, giving a measure of resistivity. An ETMT rig was developed at the National Physical Laboratories (NPL) to conduct tests with the ability to alter the load on specimen during testing, Figure 2(b).[13–15] Previous results from this type of testing showed that the change in resistance of a known volume of material (resistivity) was indicative of the internal microstructure of the specimen tested.[13–16]

Load-control allows compensation for any change in specimen geometry, such as thermal expansion, during a test. The rig is used with specimen sizes of 40 mm × 5 mm × 0.5 mm, heated at a rate of 50 °Cs^{-1} in the central region to a chosen temperature to within ±0.5 °C. The grips are held at room temperature, 22 ± 2 °C, by water-cooling at an initial distance of 22 mm apart. The resultant effect on the specimen is a temperature gradient of a known parabolic shape, Figure 2(c).[13] All tests are conducted in a controlled atmosphere of inert gas (argon) to reduce oxidation at elevated temperatures.

The rig allows the resistance of a known region of specimen to be monitored during heat treatment for a chosen temperature, while producing isochronal heat treatment of the central 22 mm of the 40 mm long specimen with a known range of temperatures. The PID control temperatures are maintained within ±0.5 °C with a measurement error of ±0.1 °C. The known volume of the heated in the centre 2 mm length where the temperature variation is less than 2 °C at 600 °C region allows resistance to be converted to resistivity. Temperature, resistance, load, and grip displacement are measured every 10 ms. The load set to 0 ± 0.1N follows small changes in the length as maintaining a zero load is required to compensate for any expansion or contraction of the test specimens when subject to heat treatment. This is taken into account when analysing the data. The measurement of grip displacement over the entire specimen reveals dimension changes in the volume of material where the resistivity is measured, Figure 2(c). Volumetric change due to thermal expansion is proportional to temperature. In this case, the region of interest is that with the greatest temperature therefore the largest change is relative to initial volume. Accordingly, an assumption is made that half the grip displacement occurs in the region of interest. Since there are no external forces, the volume changes observed will be isotropic so that the same magnitude correction can be applied to all other dimensions when calculating resistivity. The size of the volume tested is required to calculate of resistivity and the initial distance between electrical contacts, L(0), is altered by the relative change in length over time, L(t). A(t) is the correction for the change in cross-section, dependent on the isotropic assumption, which in each dimension is of the same magnitude as the change in length, see the following equation:

$$A(t) = A(0)\left(1 + \frac{L(t) - L(0)}{L(0)}\right), \tag{3}$$

where A(0) and L(0) are measurements made at the beginning of the test. Considering the measured changes in resistance and dimension, a time dependent resistivity, $\rho(t)$, can be derived for constant thermal conditions and zero load, see the following equation:

$$\rho(t) = \frac{V(t)A(t)}{I(t)L(t)}. \quad (4)$$

This describes how resistivity changes measured at high temperatures are linked to a change in microstructure.[16]

IV. RESULTS

A. Static microstructural observations

Discrete resistivity measurements conducted with a standard four-point probe technique were undertaken at temperatures of 77 K and 300 K (where the microstructure is stable) for a range of uni-modal grain size distributions, produced by heat treatment of nc nickel below a temperature of 758 K. Higher resistivity values were measured at the smallest grain sizes at both temperatures; overall, lower resistivity is measured at 77 K, Figures 3(a) and 3(b). These results display the standard deviation of the data collected in the form of error-bars and with a line of best fit to the minimal square of the residuals obtained by co-fitting both room temperature and liquid nitrogen tests through the change in proportion of grain boundary volume, Eq. (2). The microstructure in both experiments is the same, therefore, the average grain boundary width is common to both models. The two co-dependent problems are fitted using a pair of orthogonal 6-D variable space matrices and location of the minimum of the square of residuals is found taking into consideration the standard deviation of the measured data.

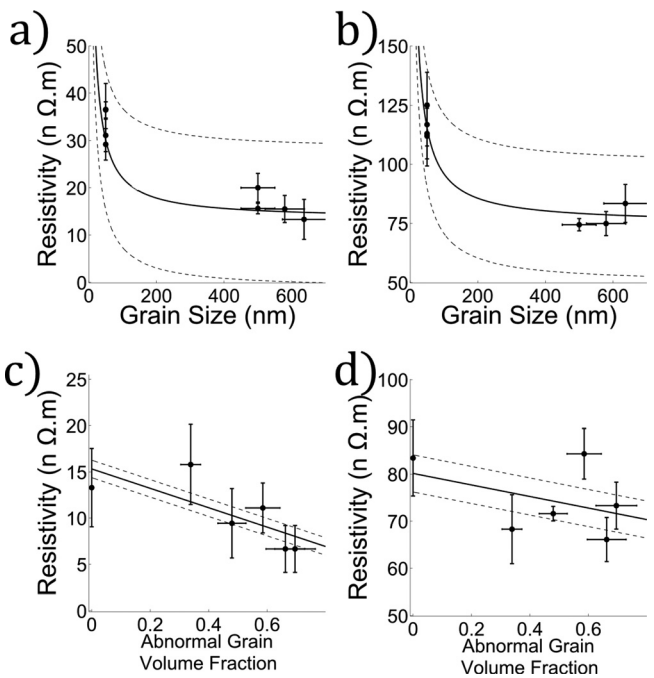

FIG. 3. (a) and (b) Show the resistivity with grain size of uni-modal microstructures co-fitted to Eq. (2) of test conducted at 77 K (a) and 300 K (b), with correlation coefficient of 0.874 and 0.931, respectively. (c) and (d) Resistivity plotted with increasing proportion of abnormal grain boundary volume of measurements at 77 K (c) and 300 K (d) fitted linearly with correlation coefficient of 0.74 and 0.81, respectively.

The result leads to values for the average grain boundary volume, and the contributions of grains, grain boundary, and temperature to resistivity, are displayed in Table I. The fit gives a resistivity due to electron-electron scattering to be zero, as expected for this current density and the resistivity of a grain interior to be zero, as expected for a perfect single crystal irrespective of temperature.

Heat treatment of this nc nickel above 758 K leads to abnormal growth from a stagnant distribution of nano-grains, therefore, the change in grain boundary volume fraction with proportion of abnormal grains is linear ($M = 1 - A$), see the following equation:

$$\begin{aligned}\rho_{total} &= M\rho_{matrix} + A\rho_{Abnormal} \\ &= \rho_{matrix} + A(\rho_{Abnormal} - \rho_{matrix}).\end{aligned} \quad (5)$$

This gives a measure of the resistivity of the two components of the microstructure, as the proportion of the two different grain size distributions changes. The data, Figures 3(c) and 3(d), show the linear fit and give the resistivity of the smaller grained, higher grain boundary proportion, matrix consistently exceeded that for the large grained abnormal distribution, Table I. The resistivity for the abnormal grain sized region is that of large grains and as such the value 67.6 ± 11.5 nΩ m is comparable with polycrystalline nickel literature value 69.9 nΩ m.[17]

B. Time resolved microstructure evolution

The microstructure of nc nickel is thermally unstable as observed by grain growth at temperatures above 573 K, therefore time resolved data logging changes in resistivity can be observed as the microstructure evolves. An ETMT rig was used to hold the test specimen under zero load by resistive heating and maintained at constant temperature through a thermocouple in a proportional integral derivative feedback loop with the applied current.[15] Measuring the current and voltage across a known volume gives resistivity *in-situ* with heat treatment. Figure 4(a) shows heat treatment at a temperature of 773 K for nc nickel against time displaying the decrease resistivity as nano-grain coarsening progresses to

TABLE I. Values calculated from fitting resistivity measurements.

	Temperature (K)		
	77	300	773
Average grain boundary width (nm)	0.61 ± 0.01	0.61 ± 0.01	0.61 ± 0.01
ρ_{ee} (nΩ m)	0	0	0
$\rho_{lattice}(T)$ (nΩ m)	13 ± 3	74 ± 8	260 ± 20
$\rho_{non-lattice}(T)$ (nΩ m)	367 ± 3	1100 ± 8	740 ± 20
ρ_{grain} (nΩ m)	0	0	0
ρ_{gb} (nΩ m)	197.04	197.04	197.04
ρ_{matrix} (nΩ m)	16 ± 4	77 ± 6	344 ± 1
$\rho_{Abnormal}$ (nΩ m)	3 ± 6	68 ± 12	316 ± 1

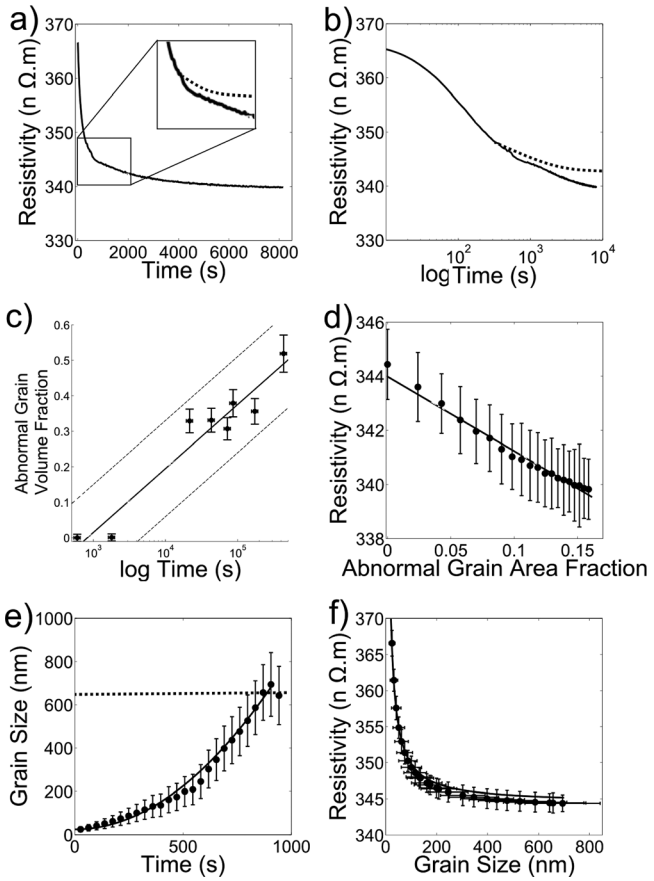

FIG. 4. (a) *In-situ* resistivity evolution over time as nc nickel is heated at 773 K, (b) resistivity plotted against log(time) displays the change in gradient as the grain growth mode shifts, both illustrate the resistivity curve due to stagnation without abnormal growth by a dashed line, (c) plot of abnormal grain volume fraction against log time of heat treatment at 773 K linearly fitted with a correlation coefficient of 0.93, (d) resistivity after 920s heat treatment plotted against abnormal grain area fraction evolution. (e) Translated result of grain size against time for grain coarsening and (f) resistivity plotted against calculated grain size.

stagnation followed by abnormal growth as observed in the static cases, the deviation in the curve is highlighted by use of a dotted line to represent the data expected to observe without abnormal growth. The change to abnormal growth can be seen clearly in Figure 4(b), where resistivity is plotted against log time, as a change in gradient. This change from grain coarsening to stagnation and the abnormal growth is observed before 1000 s. Abnormal grain volume fraction relative to time of heat treatment, from *ex-situ* heat treatments Figure 4(c), allows interpolation using a linear fit against log(time), leading to the time for first appearance of abnormal grains as 920 s. Given this linear fit, the time after 920 s can be translated into abnormal grain volume faction, leading to a plot of resistivity against abnormal grain volume faction, Figure 4(d), as in the static microstructure case the values for the matrix and abnormal grain resistivity as found, Table I. As asserted earlier, the resistivity is known to vary linearly with proportion of grain interior; combining these data with measured values from *ex-situ* heat treatments allows the measured resistivity against time in the coarsening regime to be translated into G against time, SI. As the relationship between G and grain radius is known, then the data can be translated one step further to give grain size with time, Figure 4(e). Figure 4(e) shows the grain size evolution with time during heat treatment with a fit up to 920 s with an r^2 relationship; the growth rate given by dr/dt is proportional to the grain size. Therefore, the rate of growth of the nc grains is directly related to their size, until stagnation. A final step can be taken to plot resistivity against grain size with related errors in both, Figure 4(f). The error in resistivity is measured standard deviation and the error in grain size is due to the error in the translations and as such this is a maximum as G approaches 1, where grain size is large. Plotting grain size against resistivity, Figure 4(f) allows fitting to deconvolute values for the thermal, grain, and grain boundary contributions to resistivity. As in the static microstructure case, the electron-electron scattering and grain interior scattering are zero with the value of grain boundary volume contribution constant, Table I.

This section illustrates the use of resistivity measurements at temperature to follow grain growth in a material. The steps taken in relating the time of measurement to a grain size are exhaustively covered with the use of Figure 5 for completeness. Shown in Figures 4(a) and 4(b) are the resistivity measurements with time. In accordance with Equation (2), resistivity has a linear relationship with grain interior volume, and the grain interior volume is known at two times due to *ex-situ* testing, allowing grain interior volume calculations to be interpolated along a linear path, leading to Figure 5(a). The calculated points can then be translated through the measured time-resistivity relationship resulting in Figure 5(b) where grain interior volume is calculated for the time scale of the interpolated grain growth. Finally, the relationship between grain size and grain interior volume is known from Eq. (1), Figure 5(c), allowing translation of the calculated grain interior volume into grain size resulting in the calculated Figure 4(e). The translation through the measured resistivity-time can be utilised once more to give 4(f).

V. DISCUSSION

This study shows that the microstructure of a single phase polycrystalline metal has an impact on resistivity with a sufficient magnitude in small grain size materials to be measurable as a distinct effect separate from the contribution of temperature. The deconvolution of the electrical resistivity contribution of dislocation structure is undertaken by comparison with a number of known microstructures. This temperature dependence of resistivity in high grain boundary volume fraction materials can be understood by describing the total bulk with an average grain size and an average grain boundary volume proportion associated with each grain, see Appendix.

The nc grains observed have a low density of interior dislocations and this is supported by little strain shown by electron and X-ray diffraction.[20] Therefore, via the assumption that a perfect crystal at 0 K has no resistance, the effect of lattice structures is thermally dependent. The thermal trend is in agreement with previous experimental observations and standard mechanistic modeling of the thermal-resistance profile for macro-scale polycrystalline nickel.[3,18]

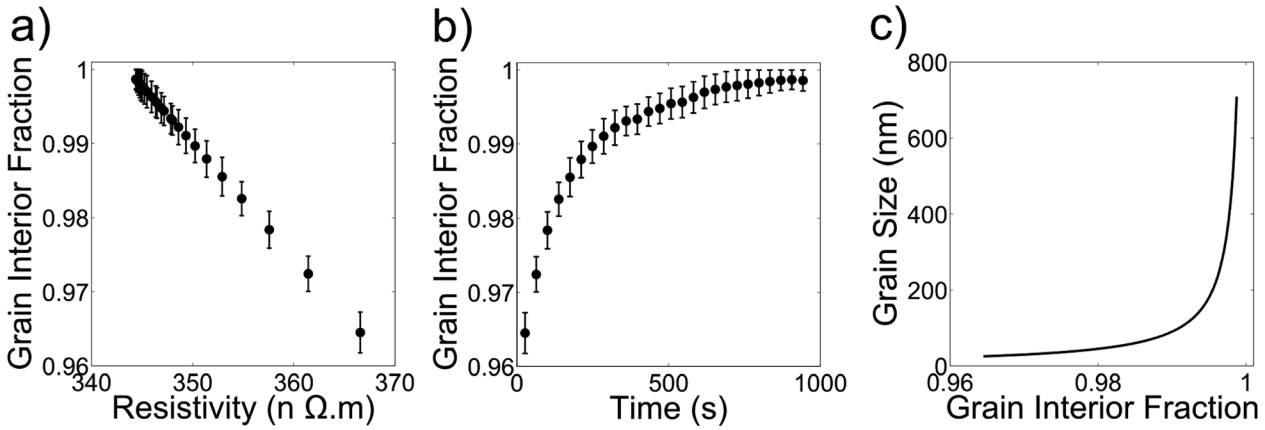

FIG. 5. (a) Shows the linear relationship between grain interior fraction and resistivity, (b) relationship of grain interior to time through resistivity, and (c) the relation of grain size to grain interior fraction.

Hence, it is important to consider in the differing proportion of increase in resistance with temperature that arises from different defect structures. The present results reveal that the proportional increase in the phonon resistivity arising from grain interiors is greater than from grain boundary volume so that an increase in temperature causes a greater reduction of electron transport through a crystalline as opposed to non-crystalline regions. This observation aligns with the presence of thermally excited vibrational modes within the lattice structure, so that the number of phonons produced thermally within a material is linked to the resistivity of the microstructure. As temperature increases the resistivity, it is necessary for measurements to be undertaken at low temperatures of periodic atomic arrangements in order to provide the greatest resolution between crystalline and non-crystalline regions in a material. Thus irrespective of the test temperature, the effect of microstructure on resistivity can be measured; the production of phonons, in turn, hinders electron transport through the material. It is important to recognise that the number of crystal defects, such as dislocations, is inversely related to the number of phonons.[4] Hence, removal of defects and grain boundaries will lead to a uniform crystal lattice thus increasing the number of phonons available.

The present work has demonstrated that it is possible to monitor the kinetics of grain coarsening in nc nickel. Moreover since the abnormal grains grown by simple consumption and replacement of the stagnant coarsened nanograin structure, it is possible to monitor the progressive change in the total volume fraction of these grains. At low temperatures where microstructure is constant, the role of scattering due to phonons is reduced, leading to a larger proportion contribution to the measured resistivity as a direct result of the dislocation structure. Since the interaction of conducting electrons with phonons is dominant at higher temperatures, the direct effects of defects are obfuscated. However, the number of the phonons present is dependent on temperature and the atomic arrangement of atoms, therefore, as observed in the single phase nickel, it is possible to link resistivity measurement with microstructure indirectly. Observation of grain coarsening *in-situ* through observation of resistivity reduction illustrates that the removal of defects through growth is a greater magnitude than the increase due to additional phonons giving rise to more phonon-electron interaction. The combined direct and in-direct relationship of resistivity to microstructure provides a valuable technique to measure grain growth in nc single phase materials.

VI. CONCLUSIONS

- The structure of nanocrystalline metals can be characterised as a ratio of grain and grain boundary volumes.
- Electrical resistivity can be used to measure a change in the proportions of grain and grain boundary volume.
- The resistivity can be measured *in-situ* with isothermal heat treatment to follow grain size evolution.
- The temporal information on change in proportion of grain boundary volume gives observation of different types of grain growth.

ACKNOWLEDGMENTS

The authors (J. Darnbrough and P. E. J. Flewitt) would like to thank EPSRC for financial support via Grant No. EP/H006729/1. NPL acknowledges the support of the UK Department of Business, Industry and Skills through the National Measurement System Materials Programme.

APPENDIX

1. 3D model of tessellating microstructure

The regular body centred arrangement of tetradecahedron is proposed by Kelvin as a solution to the question of the equal division of space by a efficient foam.[6] The arrangement as space filling grains is modified to give each tetradecahedron as a grain within another slightly larger tetradecahedron where by the difference in distance from the centre of the tetradecahedron to the face is equal to half the grain boundary width. This gives a regular arrangement of "grains," of size d and radius r, equally separated by a distance of grain boundary width, w. The relative sizes of the "grain" and "grain plus half boundary" tetradecahedrons allow the proportional volumes of grain, G, and grain boundary, B to be found.

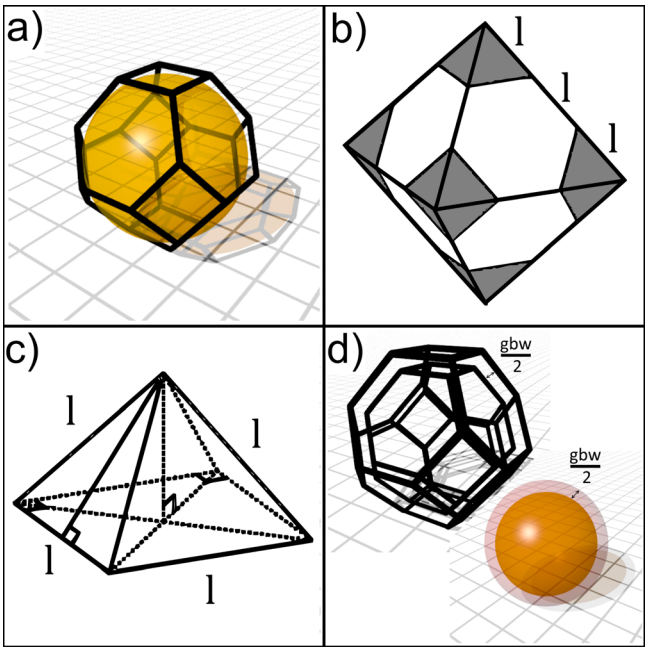

FIG. 6. a) A tetradecahedron with a sphere contained within it, b) regular truncated octahedron as a combination of square based pyramids, c) square based pyramid with equal sides and d) the relationship between Russian-doll tetradecahedrons and spheres.

Construction and application of this form of tetradecahedron with a grain boundary volume will now be considered mathematically to illustrate that the dimensionless ratio between volumes can be considered as spheres, Figure 6(a). To construct this grain arrangement, we consider a regular truncated octahedron (a tessellating tetradecahedron) combining two large square based pyramids with six smaller one taken from the points, Figure 6(b) and all have the same side length, Figure 6(c), then the volume, V_{total}, can be written as follows:

$$\begin{aligned} V_{total} &= 2V_{large} - 6V_{small} \\ &= 2\left(\frac{(3l)^3}{6}\right) - 6\left(\frac{l^3}{6}\right) \\ &= 8l^3, \end{aligned} \tag{A1}$$

where l is the side length depicted in Figures 6(b) and 6(c). The distance from the centre of the tetradecahedron to the centre of each square face, *dtf*, is the height, h, of a large pyramid minus the height of a small one, see the following equation:

$$\begin{aligned} dtf &= h_{large} - h_{small} \\ &= \frac{3l}{\sqrt{2}} - \frac{l}{\sqrt{2}} \\ &= \frac{2l}{\sqrt{2}}. \end{aligned} \tag{A2}$$

Given this distance, *dtf*, a sphere can be constructed which is contained completely within the tetradecahedron touching six faces, Figure 6(a), and with a volume that is related to the tetradecahedron by a constant, C, see the following equation:

$$\begin{aligned} V_{total} &= CV_{sphere} \\ &= C\left(\frac{4}{3}\pi r^3\right) \\ &= C\left(\frac{4}{3}\pi\left(\frac{2l}{\sqrt{2}}\right)^3\right) \\ &= C\left(\frac{4}{3}\pi\frac{1}{2^{\frac{3}{2}}}V_{total}\right) \\ C &= \frac{3\sqrt{2}}{2\pi}. \end{aligned} \tag{A3}$$

The size of the tetradecaheda can now be related in radii of the internal spheres so the incremental increase in volume attributed to half the grain boundary width is defined, Figure 6(d). The proportional volume of grain interior to total is given by Eq. (A4) as the larger tetradecahedron tessellates what is contained is indicative of the whole. Figure 7(a) shows 2D section through the 3D grain tessellation containing a grain boundary width

$$\begin{aligned} V_{total} &= V_{tetradecahedron} = CV_{shpere} = C\frac{4\pi}{3}\left(r + \frac{w}{2}\right)^3 \\ V_{grain} &= CV_{shpere} = C\frac{4\pi}{3}r^3 \\ G &= \frac{V_{grain}}{V_{total}} \\ &= \frac{r^3}{\left(r + \frac{w}{2}\right)^3}. \end{aligned} \tag{A4}$$

This relationship allows the dichotomy of the microstructure, divided into ordered grain regions and reduced order grain boundary regions, and the ratio of those two to

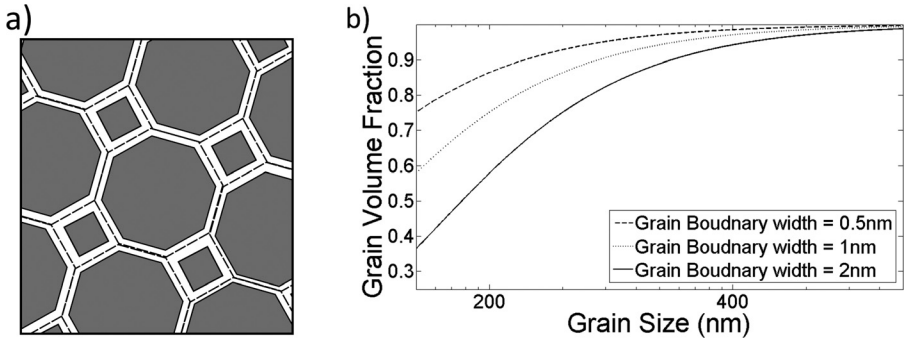

FIG. 7. (a) Specific 2D section through a 3D tessellated grain structure with grain volume highlighted in gray and (b) plot of the predicted showing change in grain volume with grain size, Eq. (1).

be represented through an average grain size and an average grain boundary width. The relationship between grain interior volume and grain size, d, for various grain boundary widths, w, is shown in Figure 7(b). Here, the difference given by grain boundary width becomes indistinguishable once the grain size is greater than 400 nm, however at small grain sizes, the effect is pronounced; the insert for the grain size $\leq$100 nm highlights the initial 50 nm grain size of the nc nickel used in this investigation.

[1]T. Hanlon, Y.-N. Kwon, and S. Suresh, Scr. Mater. **49**, 675 (2003).
[2]C. C. Koch, "Nanostructured materials: An overview," in *Bulk Nanostructured Materials* (Wiley-VCH Verlag GmbH and Co. KGaA, 2009), pp. 1–20.
[3]N. Mott, Proc. R. Soc. London, Ser. A **153**, 699 (1936).
[4]J. M. Ziman, *Electrons and Phonons: The Theory of Transport Phenomena in Solids* (Oxford University Press, 1960).
[5]A. F. Mayadas and M. Shatzkes, Phys. Rev. B **1**, 1382 (1970).
[6]S. W. Thomson, Philos. Mag. Ser. 5 **24**, 503 (1887).
[7]J. E. Darnbrough, S. Mahalingam, and P. E. J. Flewitt, J. Phys.: Conf. Ser. **371**, 012076 (2012).
[8]R. A. Millikan, *Elements of Electricity: A Practical Discussion of the Fundamental Laws and Phenomena of Electricity and Their Practical Applications in the Business and Industrial World* (American Technical Society, 1917).
[9]T. J. Seebeck, Abh. K. Akad. Wiss Berlin 289–346 (1821).
[10]C. Suryanarayana, Int. Mater. Rev. **40**, 41 (1995).
[11]C. S. Smith, Met. Technol. **15**, 37 (1948).
[12]H. Gleiter, Prog. Mater. Sci. **33**, 223 (1989).
[13]S. Pahlavanyali, A. Rayment, B. Roebuck, G. Drew, and C. Rae, Int. J. Fatigue **30**, 397 (2008).
[14]B. Roebuck, M. Loveday, and M. Brooks, Int. J. Fatigue **30**, 345 (2008).
[15]B. Roebuck, D. C. Cox, and R. C. Reed, in *Superalloys 2004*, edited by K. A. Green, T. M. Pollock, H. Harada, T. E. Howson, R. C. Reed, J. J. Schirra, and S. Walston (The Minerals, Metals and Material Society, 2004), p. 523.
[16]B. Roebuck, D. Cox, and R. Reed, Scr. Mater. **44**, 917 (2001).
[17]S. Mahalingam, P. Flewitt, and J. Knott, Mater. Sci. Eng., A **564**, 342 (2013).
[18]R. Kumara, L. Nicolab, and E. V. der Giessen, Mater. Sci. Eng., A **527**, 7 (2009).
[19]J. Sun, Y. Zhang, G. Rao, Y. Liu, and S. Liu, "Resistance behaviuor of nanocrystal nickel," Mater. Sci. Technol. **9**, 185 (1993).
[20]J. E. Darnbrough and P. E. J. Flewitt, "Growth of abnormal planar faceted grains in nanocrystalline nickel containing impurity sulphur," Acta Materialia **79**, 421–433 (2014).
[21]J. Friedel and J. M. Ziman, *The Physics of Metals* (Cambridge University Press, London, 1969), p. 340.